Arch. Mech., 41, 1, pp. 133–155, Warszawa 1989

Application of internal time and internal variable theories of plasticity to complex load histories (*)

W. BROCKS and J. OLSCHEWSKI (BERLIN)

Two constitutive models for metals at elevated temperatures, i.e., Chaboche's model of internal variables and the endochronic theory of Valanis are compared to study the efficiency and limitations of these models in the case of complex load histories. Several numerical tests for strain-controlled homogenous axial torsional loading have been carried out i.e., out-of-phase loadings, stair tests and load paths with abrupt changes of the loading direction. The material constants are determined from hot tension and low-cycle-fatigue tests of the alloy Nimonic PE16. Furthermore, the inelastic behaviour of a notched cylindrical specimen under cyclic loading is studied and the results of the two models are discussed. To this end, both models have been implemented into a finite element program. The variation of stresses and strains in the net section of the notched bar subjected to a random cyclic loading in the transient regime of the material will be presented.

Porównano ze sobą dwa modele metali przy podwyższonych temperaturach, tj. model Caboche'a o zmiennych wewnętrznych oraz endochroniczną teorię Valanisa; porównanie to miało na celu stwierdzenie efektywności ich stosowania oraz ewentualnych ograniczeń przy zastosowaniu do przypadków złożonych historii obciążenia. Wykonano szereg prób numerycznych odpowiadających skręcaniu. Stałe materiałowe określono z prób rozciągania oraz zmęczenia niskocyklowego przeprowadzonych na stopie Nimonic PE16. Przeanalizowano również efekty niesprężyste w cylindrycznej próbce z karbem w odniesieniu do obu rozważanych modeli. W tym celu wprowadzono oba modele do programu metody elementów skończonych.

Сравнены с собой две модели металлов при повышенных температурах, т. е. модель Кабоша с внутренними переменными и эндохроническая теория Валяниса; это сравнение имело целью констатировать эффективность их применения и обнаружить вероятные ограничения, при применении к случаям сложных историй нагружения. Проведен ряд численных испытаний отвечающих скручиванию. Материальные постоянные определены из испытаний растяжениями и низкоцикловой усталости, проведенных на сплаве Нимоник PE16. Проанализированы тоже неупругие эффекты в циклическом образце с надрезом по отношению к обоим рассматриваемым моделям. С этой целью обе модели введены в программу метода конечных элементов.

Notations

$\delta(z)$ Dirac function,
$\bar{\varepsilon}$ effective strain,
$f(\zeta)$ hardening function (Valanis),
Φ^* measure of nonproportionality,
G elastic shear modulus,
H hardening modulus,
Λ strain path-dependent integral,
p accumulated effective plastic strain,
$\dot{p}$ effective plastic strain rate,

(*) Presented at the 4th Polish-German Symposium on Mechanics of Inelastic Media and Structures, Mogilany (Poland), September 1987.

$\varrho(z)$ kernel in Valanis' constitutive integral equation,
$\bar{\sigma}$ von Mises effective stress,
σ_{y0} yield strength in uniaxial tension test,
z intrinsic time (Valanis),
ζ arc length in the space of plastic strains,
$\mathbf{A} = \alpha_{ij}\mathbf{e}_i\mathbf{e}_j$ Cauchy back-stress tensor,
$\mathbf{A}'$ deviator of Cauchy back-stress tensor,
$\overset{\langle 4\rangle}{\mathbf{C}}$ fourth order elasticity tensor,
$\dot{\mathbf{E}} = \dot{\mathbf{E}}_e + \dot{\mathbf{E}}_p$ strain rate tensor (total, elastic, plastic),
$\mathbf{H}_1$ strain history tensor (Valanis),
$\mathbf{S} = \sigma_{ij}\mathbf{e}_i\mathbf{e}_j$ Cauchy stress tensor,
$\mathbf{S}'$ deviator of Cauchy stress tensor,
$||\mathbf{T}|| = \sqrt{\mathbf{T}\cdot\cdot\mathbf{T}} = \sqrt{t_{ij}t_{ij}}$ Euclidean norm of a tensor $\mathbf{T}$.

1. Introduction

IN RECENT years material research and constitutive modelling in the high-temperature range have become an increasingly important field of research. On one hand, advances in experimental mechanics and, in particular, servo-controlled testing have provided novel and comprehensive test data on both the micro and the macro level. On the other hand great progress in computational mechanics has made it possible to introduce more and more sophisticated constitutive models into the solution of complex initial boundary value problems.

Despite the fact, that one can find a great number of inelastic constitutive equations in the literature, the question regarding what kind of model is suitable for inelastic analysis is still open. Therefore the demand for an appropriate constitutive equation which is able to characterize the three-dimensional material response for a broad variety of load histories in the high temperature range continues.

The present paper numerically compares two current constitutive models for metals at elevated temperatures. The models chosen for this work are CHABOCHE'S model [1, 2] and a model based on the endochronic theories of VALANIS [3, 4], VALANIS and FAN [5, 6] and WATANABE and ATLURI [7, 8]. The first model is a member of the class of internal variable theories whereas the second model, based on an intrinsic time measure, represents an alternative way of modelling inelastic material behaviour. A summary of the basic equations of the two models are given in Sect. 2. The primary objective of this work is to study the predictive capabilities of these models in the case of complex loading histories, e.g., for nonproportional load paths and load histories with varying strain amplitudes. Therefore the rate-independent versions of the two models have been used for convenience in the present study.

The background for this study is the experimentally observed behaviour that cyclic hardening is considerably higher under nonproportional loadings when compared to proportional loadings, LAMBA and SIDEBOTTOM [9], KANAZAWA and MILLER [10], CAILLETAUD *et al.* [11], MCDOWELL [12], TANAKA *et al.* [13], BENALLAL and MARQUIS [14]. Because of the fact that the additional hardening is generally dependent on the shape of

the loading path, the two models have been applied to a broad variety of biaxial non-proportional straihings generated in smooth tubular tension-torsion specimens. Examples of the numerically carried out tension-torsion experiments are out-of-phase loadings, stair-tests and loading paths with abrupt changes of the loading direction. An overview of the numerical tests analyzed in the present study is given in Sect. 3. Furthermore, an attempt is made to classify the nonproportional tests with respect to their nonproportionality.

Beside these tests which led to homogeneous states of stresses and strains, the problem of a circumferentially notched specimen subject to a load history with varying strain amplitudes has also been investigated, in particular the elasto-plastic stress-strain state in the vicinity of the notch root. For that purpose, the two mentioned constitutive models have been implemented in the FE computer code ADINA [15]. According to the work of WATANABE and ATLURI, the present endochronic theory has been implemented in the same elasto-plastic algorithm which is usually used for classical incremental theories.

The material constants of both models are determined from hot-tension and low-cycle-fatigue tests using the high-temperature alloy Nimonic PE16. All tests are carried out at 650°C under a strain rate of $\dot{\varepsilon} = 4 \cdot 10^{-3}\ \mathrm{s}^{-1}$.

2. Basic equations of internal variable theory and endochronic theory

The classical incremental theory of rate-independent isothermal plasticity consists of the following elements:

1) an additive decomposition of the total strain rate (or increment) into an elastic and plastic part

$$\dot{\mathbf{E}} = \dot{\mathbf{E}}_e + \dot{\mathbf{E}}_p; \tag{2.1}$$

2) a constitutive equation for the elastic strain rate (Hooke's law)

$$\dot{\mathbf{S}} = \overset{\langle 4 \rangle}{\mathbf{C}} \cdot \cdot \dot{\mathbf{E}}_e; \tag{2.2}$$

3) a yield condition which outlines the set of elastic stress states, e.g., the Huber-Mises condition

$$F(\mathbf{S}, \mathbf{A}, \varkappa) = \frac{1}{2}(\mathbf{S}'-\mathbf{A}') \cdot \cdot (\mathbf{S}'-\mathbf{A}') - \frac{1}{3}\varkappa^2(p) = 0; \tag{2.3}$$

where p is the accumulated effective plastic strain

$$p = \int_0^t \sqrt{\frac{2}{3}\dot{\mathbf{E}}_p \cdot \cdot \dot{\mathbf{E}}_p}\, dt, \tag{2.4}$$

and, by a geometrical interpretation in the stress hyperspace, the tensor $\mathbf{A}$ describes the translation of the centre of the yield surface (kinematic hardening) and the scalar $\varkappa$ its expansion (isotropic hardening);

4) hardening rules for the "internal variables" $\mathbf{A}$ and $\varkappa$ in the form of evolution equations

$$\dot{\mathbf{A}} = \dot{\bar{\mathbf{A}}}(\mathbf{S}, \mathbf{E}_p, \mathbf{A}, \varkappa, \dot{\mathbf{S}}, \dot{\mathbf{E}}_p), \tag{2.5}$$
$$\dot{\varkappa} = \dot{\bar{\varkappa}}(\mathbf{S}, \mathbf{E}_p, \mathbf{A}, \varkappa, \dot{\mathbf{S}}, \dot{\mathbf{E}}_p);$$

5) a constitutive equation for the plastic strain rate called the "flow rule" (or normality rule)

$$\dot{\mathbf{E}}_p = \begin{cases} \dot{\lambda}(\partial F/\partial \mathbf{S}) & \text{for} \quad F = 0 \quad \text{and „loading''}, \\ 0 & \text{for} \quad F < 0 \quad \text{or „unloading''}; \end{cases} \tag{2.6}$$

6) the loading/unloading condition for a stress increment starting from a yield state $F = 0$

$$\dot{\mathbf{S}} \cdot \cdot (\partial F/\partial \mathbf{S}) \begin{cases} > 0 & \text{loading}, \\ = 0 & \text{neutral loading}, \\ < 0 & \text{unloading}. \end{cases} \tag{2.7}$$

Various models have been developed within this framework which differ by their evolution equations (2.5) for isotropic and kinematic hardening, mainly. CHABOCHE *et al.* [1, 2], e.g., proposed the equations given in the left row of Table 1.

A basically different approach to plasticity was given by VALANIS [3, 4] who proposed a constitutive equation

$$\mathbf{S}' = 2G \int_0^z \varrho(z-\bar{z}) \frac{d\mathbf{E}_p}{d\bar{z}} d\bar{z} \tag{2.8}$$

which related the present stress tensor to the whole plastic strain history. The "intrinsic time" measure z of this history is defined through

$$dz = \frac{d\zeta}{f(\zeta)}, \quad f(\zeta) > 0, \quad f(0) = 1, \tag{2.9}$$

where $d\zeta$ is the incremental arc length in the space of plastic strain

$$d\zeta = (d\mathbf{E}_p \cdot \cdot \, d\mathbf{E}_p)^{1/2} \tag{2.10}$$

which, in this definition, differs from the effective plastic strain increment dp just by a factor of $\sqrt{2/3}$. Apparently, Valanis' "endochronic theory" does not need a yield condition like Eq. (2.1) but his constitutive equation (2.8) can easily be rewritten in a form which shows a complete analogy to the von Mises yield condition and the evolution equations for isotropic and kinematic hardening. VALANIS and FAN [5, 6] proposed an algebraic expression of three exponential terms for the kernel $\varrho(z)$ which has been slightly modified by WATANABE and ATLURI [7, 8]:

$$\varrho(z) = \varrho_0 \delta(z) + \varrho_1(z), \tag{2.11}$$
$$\varrho_1(z) = \sum_1^3 c_k e^{-\alpha_k z}.$$

Introducing this expression into Eq. (2.8) and taking its Euclidean norm, one obtains

$$\|\mathbf{S}' - \mathbf{A}'\| = 2G\varrho_0 f(\zeta) \tag{2.12}$$

Table 1. Comparison of the basic constitutive equations in the internal variable and the endochronic theories of plasticity, respectively, [8].

Internal variable theory	Endochronic theory
yield condition $F(\sigma_{ij}, \alpha_{ij}, \varkappa, \theta) = 0$ internal variables $\alpha_{ij}, \varkappa$ $p = \int_0^t \dot{p}\,dt,\ \dot{p} = \sqrt{\frac{2}{3}}\,\|\dot{\mathbf{E}}_p\|$ von Mises $\|\mathbf{S}'-\mathbf{A}'\| - \sqrt{\frac{2}{3}}\,\varkappa(p) = 0$	*constitutive eq.* $\mathbf{S}' = 2G\int_0^z \varrho(z-\bar{z})\frac{d\mathbf{E}_p}{d\bar{z}}\,d\bar{z}$ intrinsic time $d\zeta = \|d\mathbf{E}_p\|$ $dz = \frac{d\zeta}{f(\zeta)},\ f(\zeta) \geqslant 0,\ f(0) = 1$ kernel $\varrho(z) = \varrho_0\delta(z) + \varrho_1(z)$ $\|\mathbf{S}'-\mathbf{A}'(z)\| = 2G\varrho_0 f(\zeta)$
evolution equations (Chaboche) *isotropic hardening* $\varkappa(p) = \varkappa_\infty + (\varkappa_0 - \varkappa_\infty)e^{-bp}$ $\varkappa_0 = \varkappa(0) = \sigma_{y0}$ $\dot{\varkappa}(p) = b(\varkappa_\infty - \varkappa(p))\dot{p}$ *kinematic hardening* $\mathbf{A} = \sum_{i=1}^{3}\mathbf{A}_i$ $\dot{\mathbf{A}} = \sum_{i=1}^{2} c_i(a_i\dot{\mathbf{E}}_p - \dot{p}\mathbf{A}_i) + c_3\dot{\mathbf{E}}_p$	*hardening rules* (Valanis) $f(\zeta) = 1 + a\tanh(b\zeta)$ $f(0) = 1,\quad \varrho_0 = \sqrt{\frac{2}{3}}\,\frac{\sigma_{y0}}{2G}$ $\varrho_1(z) = \sum_{k=1}^{3} c_k e^{-\alpha_k z}$ $\mathbf{A}(z) = 2G\int_0^z \varrho_1(z-\bar{z})\frac{d\mathbf{E}_p}{d\bar{z}}\,d\bar{z} = \sum_{k=1}^{3}\mathbf{A}_k$ $d\mathbf{A}(z) = 2G\{\varrho_1(0)d\mathbf{E}_p + \mathbf{H}_1(z)\,dz\}$
flow rule (normality rule) $\dot{\mathbf{E}}_p = \frac{1}{H}\,\frac{(\mathbf{S}'-\mathbf{A}')\cdot\cdot\dot{\mathbf{S}}}{2/3\varkappa^2}(\mathbf{S}'-\mathbf{A}')$ $= \frac{2G(\mathbf{S}'-\mathbf{A}')\cdot\cdot\dot{\mathbf{E}}}{2/3\varkappa^2\,(H+2G)}(\mathbf{S}'-\mathbf{A}')$ $H = \frac{2}{3}\,\frac{d\sigma}{d\varepsilon_p}$	*incremental formulation of constitutive eq.* $\dot{\mathbf{E}}_p = \frac{2G}{2/3\varkappa^2}\,\frac{(\mathbf{S}'-\mathbf{A}')\cdot\cdot\dot{\mathbf{E}}}{H+2G}(\mathbf{S}'-\mathbf{A}')$ $H = 2G\left\{\varrho_1(0) + \frac{\varrho_0}{\sigma_{y0}^2 f^2}(\mathbf{S}'-\mathbf{A}')\cdot\cdot\mathbf{H}_1 + 2\varrho_0\frac{df}{dz}\right\}$ $\mathbf{H}_1(z) = \int_0^z \left\{\frac{d\varrho_1}{dz}\right\}\Big\|_{(z-\bar{z})}\frac{d\mathbf{E}_p}{d\bar{z}}\,d\bar{z}$

if the tensor $\mathbf{A}$ is defined by

$$\mathbf{A}(z) = 2G\int_0^z \varrho_1(z-\bar{z})\frac{d\mathbf{E}_p}{d\bar{z}}\,d\bar{z} = 2G\sum_{k=1}^{3} c_k\int_0^z e^{-\alpha_k(z-\bar{z})}\,d\bar{z} = \sum_{k=1}^{3}\mathbf{A}_k. \tag{2.13}$$

We may now look at Eq. (2.12) as a yield condition and, especially, identify the constant $2G\varrho_0$ with $\varkappa_0$ or, physically, with the uniaxial yield strength σ_{y0} and the scalar hardening function $2Gf(\zeta)$ of the endochronic theory with the isotropic hardening variable $\varkappa(p)$. The tensor $\mathbf{A}'$ given by the integral equation (2.13) represents the kinematic hardening which depends on the whole strain history.

The analogies between the two concepts of internal variables and internal time, respectively, are continued if we differentiate Eq. (2.8) and thus obtain the incremental form of the endochronic constitutive equation which originates from VALANIS and FAN [5]. The plastic strain increment appears to meet the normality rule of the classical incremental theory.

Because of these analogies, summarized in Table 1 and first considered by WATANABE and ATLURI, it is possible to easily introduce the concept of internal time in a nonlinear finite element program basing on an incremental formulation as, e.g., ADINA [15]. Some results of finite element (FE) calculations utilizing both theories will therefore be presented in Sect. 4.2. On the other hand, due to the same reason one may expect that no fundamental differences will be observed in the stress-strain behaviour described by the two models, provided that the identification of the different material parameters has been done properly. This presumption has been verified by various strain-controlled calculations of axial/torsional loadings reported in Sect. 4.1. In these calculations, the original equations of CHABOCHE and VALANIS have been integrated [16, 17] instead of the incremental formulation used in the FE formulation. The integration of the constitutive equation (2.8) appeared to be very sensitive to the incrementation of the strain path. Quite different results may be obtained if the number of steps for the time integration is chosen too small.

3. Overview and classification of nonproportional loading paths

In view of the experimentally observed material behaviour of strain-path-dependent hardening, a classification of various nonproportional tests based on the amount of additional hardening was given by BENALLAL and MARQUIS [14]. This represents an attempt to define the degree of nonproportionality of a loading path. It was shown in this classification that all nonproportional loading paths will lie between the in-phase and the 90° out-of-phase loading.

In the present paper a path-dependent integral proposed by MCDOWELL [18] is used to obtain an estimate of the degree of nonproportionality of the loading path. A plastic strain based measure which is applicable to all types of nonproportional loading paths has been defined as

$$\Phi^* = \frac{\pi}{\pi-2}\left|\frac{\pi}{\pi-2} - \left|\Lambda - \frac{2}{\pi}\right|\right|, \tag{3.1}$$

where

$$\Lambda = \frac{1}{\int ||\dot{\mathbf{E}}_p||\,dt}\int_{t_B}^{t} |\mathbf{N}\cdot\cdot\,\dot{\mathbf{E}}_p|dt \tag{3.2}$$

and $\mathbf{N} = \mathbf{E}_p^*/||\mathbf{E}_p^*||$. $\mathbf{E}_p^*$ is the plastic strain tensor at maximum value of $||\mathbf{E}_p^*||$ in a given block of loading. The time at the initiation of the current loading block is denoted by t_B. Λ represents the component of the plastic strain rate in the maximum plastic strain direction averaged by the plastic strain.

The calculation of Φ^* requires the plastic strain history. In the present investigation the computation of Φ^* has been employed on total strain which does not lead to serious errors.

It can be shown that $\Phi^* = 0$ for proportional loading and $\Phi^* = 1$ for 90° out-of-phase sinusoidal, axial-torsional loading with a ratio of $\gamma_a/\varepsilon_a = \sqrt{3}$.

An overview of the loading paths analyzed in the present work and the corresponding estimate of the degree of nonproportionality is given in Table 2. In every loading path, illustrated by its shape, the maximum equivalent total strain has been kept constant and set equal to 0.5%. The predicted material response, i.e., the cyclic hardening characterized by the maximum equivalent stress obtained after the 5th cycle, is also given in Table 2. Looking at the path-dependent integral (3.2), it can be stated that Λ yields always to the same value if the angle between $\mathbf{N}$ and $\mathbf{E}_p$ remains constant along the loading path as in the cases of LIN1, LIN2 and the stair-tests. Thus Φ^* fails to differentiate the various stair-tests with respect to their varying degree of out-of-phase hardening as it was shown by Benallal and Marquis for 316 stainless steel.

Table 2. Classification of various nonproportional loading paths with respect to the path-dependent parameter Φ^* [12] and the maximum equivalent stress obtained after the 5th cycle (max. eq. total strain = 0.5%).

	LCF1	LCF3	LIN1	LIN2	LIN3	STA01	STA02	STA04	STA32	SIN30	SIN60	SIN90
												
Φ^*	0	0	0.806	0.806	0.624	0.806	0.806	0.806	0.806	0.116	0.232	1
$\bar{\sigma}_V$	577	588	560	552	558	845	623	594	589	588	595	644
$\bar{\sigma}_C$	587	597	645	640	625	618	607	603	602	600	622	677

4. Results

4.1. Homogeneous stress states (σ, τ)

Table 2 defines a number of different strain-controlled axial torsional experiments and classifies them with respect to their degree of nonproportional loading by a scalar Φ^*. These strain paths have been taken to check the behaviour of the Chaboche and the Valanis model.

The evolution equations for $\varkappa(p)$ and $\mathbf{A}(p)$ of the Chaboche model and the hardening function $f(\zeta)$ and the kernel $\varrho(z)$ of the Valanis model are described in Table 1. The material parameters of the respective functions were adopted to a hot tension and a LCF test of the nickel based alloy PE16 [19]. Both tests were carried out at 650°C and a strain rate of $\dot{\varepsilon} = 10^{-3}\,\mathrm{s}^{-1}$, the LCF test with a strain amplitude of $\varepsilon_a = 0.0258$. For the Valanis model, the fitting process described by VALANIS and FAN [6] was used for the kernel and the hardening function. The material data are summarized in Table 3. All the calculated processes meet the condition that the effective total strain

$$\bar{\varepsilon} = \sqrt{\varepsilon^2 + \gamma^2/3} \tag{4.1}$$

does not exceed 0.005.

Table 3. Material parameters of PE16 for the incremental constitutive models of Chaboche and Valanis used in the FE calculations

Chaboche			Valanis		
parameter	SI-unit	value	parameter	SI-unit	value
E	MPa	150000	E	MPa	150000
ν	—	0.3	ν	—	0.3
$\varkappa_0 = \sigma_{y0}$	MPa	425	ϱ_0	—	0.00327
$\varkappa_\infty$	MPa	647	a	—	0.3
b	—	15	b	—	10
a_1	MPa	87.3	c_1	—	1.879
a_2	MPa	200	c_2	—	0.133
c_1	—	3570	c_3	—	0.042
c_2	—	7	α_1	—	4749
c_3	MPa	3000	α_2	—	550
			α_3	—	1.39

Figures 1 to 7 show the material responses of Chaboche's and Valanis' model, labelled by CH and VA, respectively, in the (σ, τ) plane during one loading cycle of
three tests with abrupt changes of the loading directions (LIN1, LIN2, LIN3),
three stair tests (STA01, STA02, STA04) and
one out-of-phase test (SIN30).

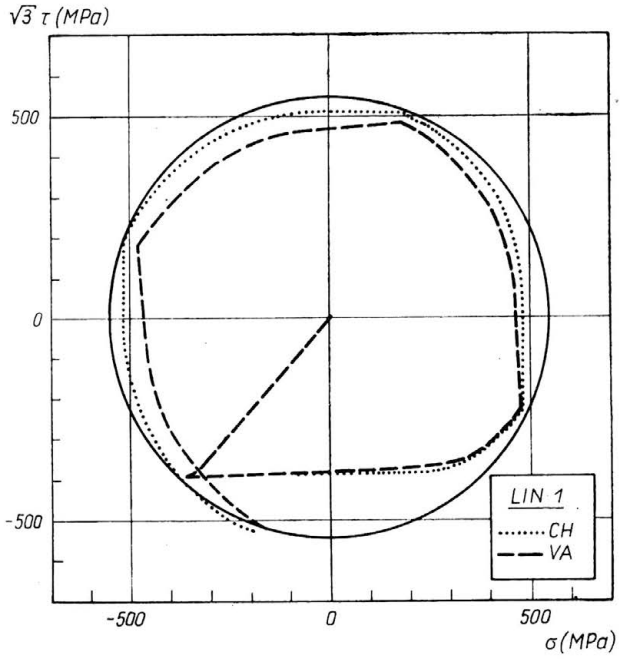

FIG. 1. Comparison of Chaboche's (CH) and Valanis' (VA) (σ,τ)-response to the first cycle of a strain controlled homogeneous axial torsional test, load path LIN 1.

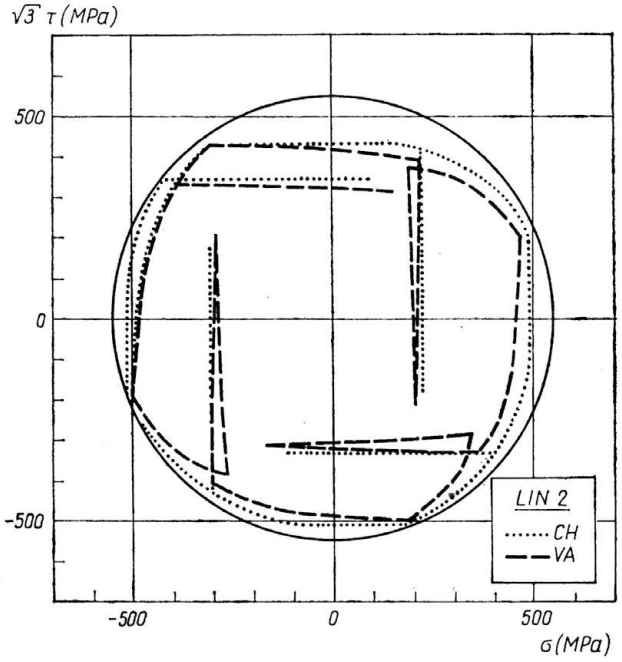

FIG. 2. Comparison of Chaboche's (CH) and Valanis' (VA) (σ,τ)-response to the first cycle of a strain controlled homogeneous axial torsional test, load path LIN 2.

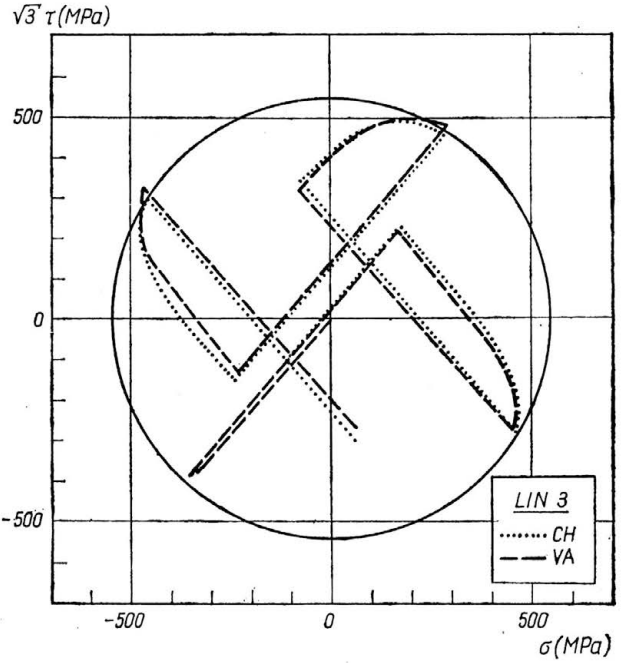

FIG. 3. Comparison of Chacoche's (CH) and Valanis' (VA) (σ,τ)-response to the first cycle of a strain controlled homogeneous axial torsional test, load path LIN 3.

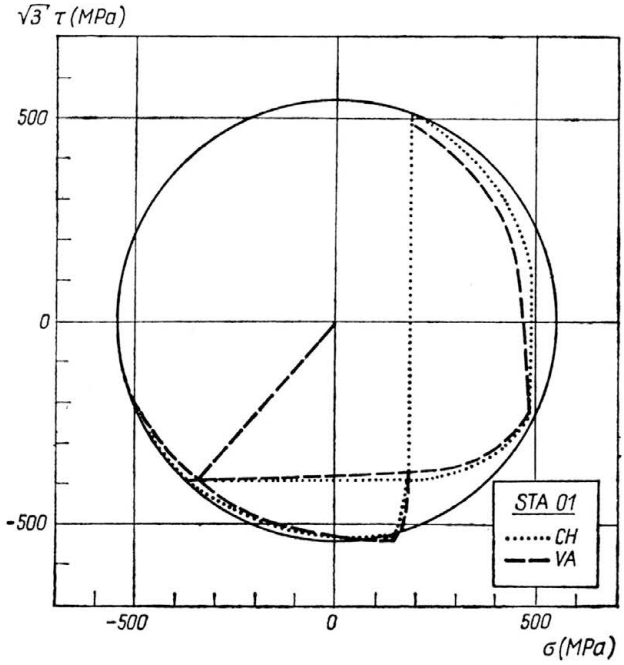

FIG. 4. Comparison of Chaboche's (CH) and Valanis' (VA) (σ,τ)-response to the first cycle of a strain controlled homogeneous axial torsional test, load path STA01 (stair test).

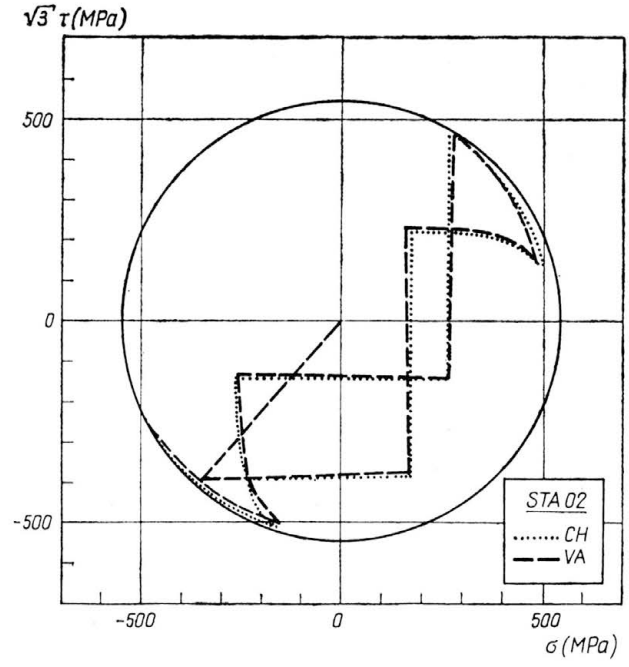

FIG. 5. Comparison of Chaboche's (CH) and Valanis' (VA) (σ,τ)-response to the first cycle of a strain controlled homogeneous axial torsional test, load path STA02 (stair test).

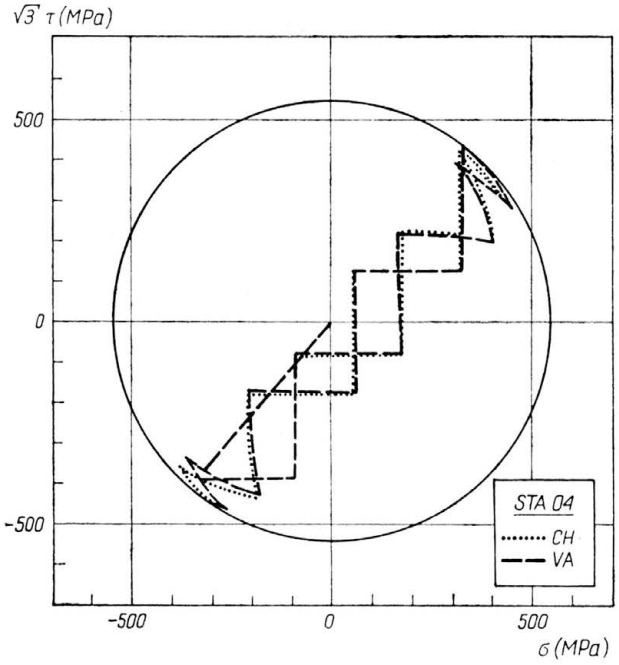

FIG. 6. Comparison of Chaboche's (CH) and Valanis' (VA) (σ,τ)-response to the first cycle of a strain controlled homogeneous axial torsional test, load path STA04 (stair test).

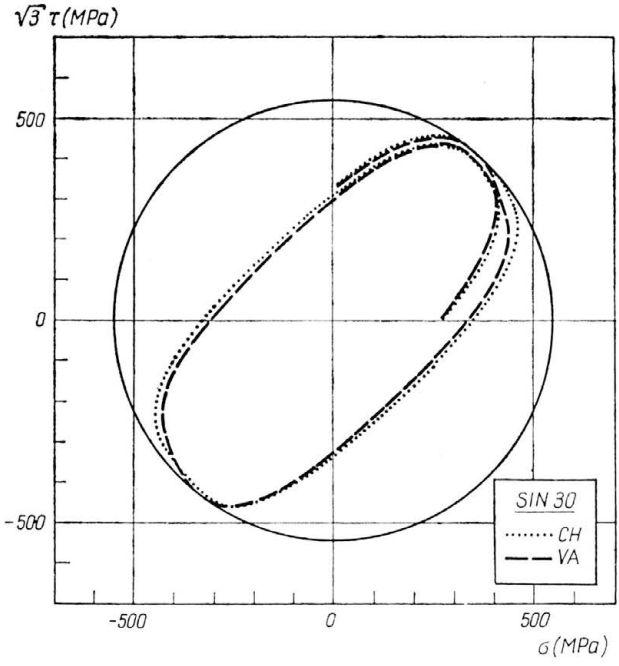

FIG. 7. Comparison of Chaboche's (CH) and Valanis' (VA) (σ,τ)-response to the first cycle of a strain controlled homogeneous axial torsional test, load path SIN30 (out-of-phase loading).

The effective stress

$$\bar{\sigma} = \sqrt{\sigma^2 + 3\tau^2} \tag{4.2}$$

which has been reached after the first cycle of a comparative LCF tension test under $\varepsilon_a = 0.005$ is represented by a circle of the radius $\sigma = 547$ MPa in these figures. Thus it is easy to see whether the strain hardening reached after one cycle of different nonproportional loadings depends on the strain path and differs between the two constitutive models. In addition, Figs, 8 and 9 show the stress-strain curves, $\sigma(\varepsilon)$ and $\tau(\gamma)$, for the out-of-phase

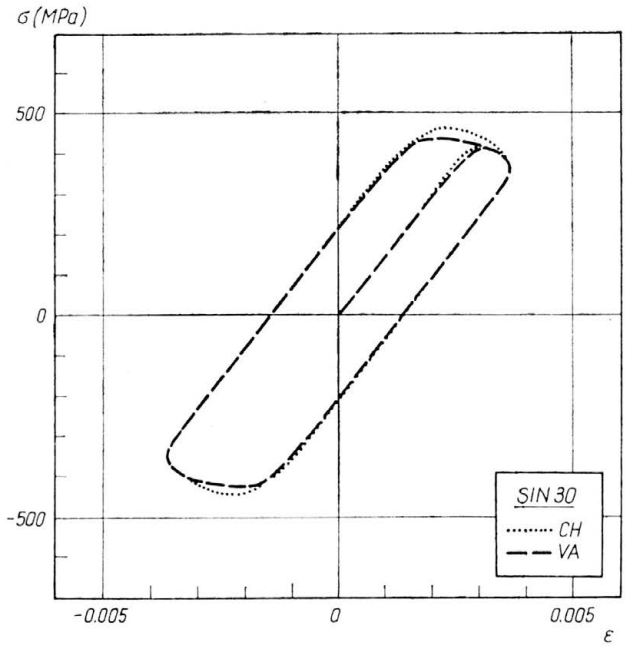

FIG. 8. Comparison of Chaboche's (CH) and Valanis' (VA) $\sigma(\varepsilon)$-curve for the first cycle of a strain controlled homogeneous axial torsional test, load path SIN30 (out-of-phase loading).

loading SIN30. As the mathematical functions which are used to describe the strain and cyclic hardening of the material differ between the Chaboche and the Valanis model, the determination of "material properties" from experimental data is rather a procedure of curve fitting and thus the parameters used for the two models are different and not directly comparable. This will probably explain some of the minor differences which can be observed with respect to the hardening behaviour in Figs. 1 to 9. Alltogether, no significant differences between the capabilities of the two models to predict the material behaviour under complex load histories can be found in the first loading cycle.

This may become different if more cycles are considered, as it is done in Table 2. Some of the loading paths show a significant difference of the two models with respect to the effective stress which is reached after five cycles. The greatest difference exists for the stair

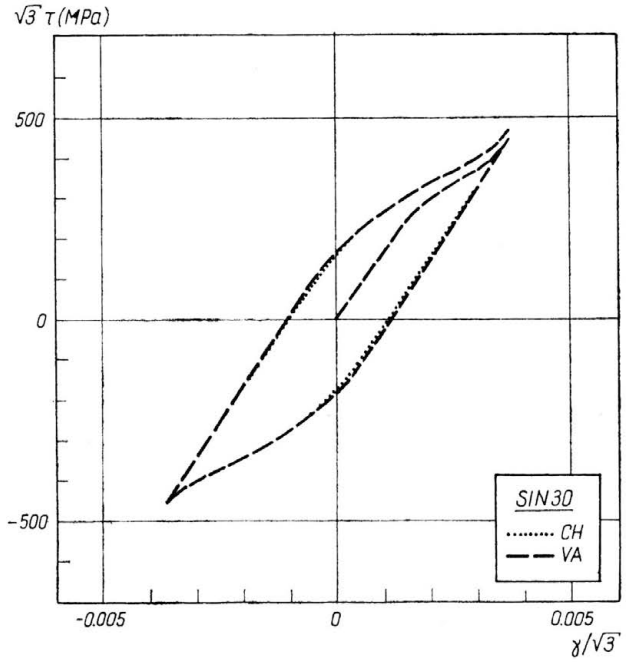

FIG. 9. Comparison of Chaboche's (CH) and Valanis' (VA) $\tau(\gamma)$-curve for the first cycle of a strain controlled homogeneous axial torsional test, load path SIN30 (out-of-phase loading).

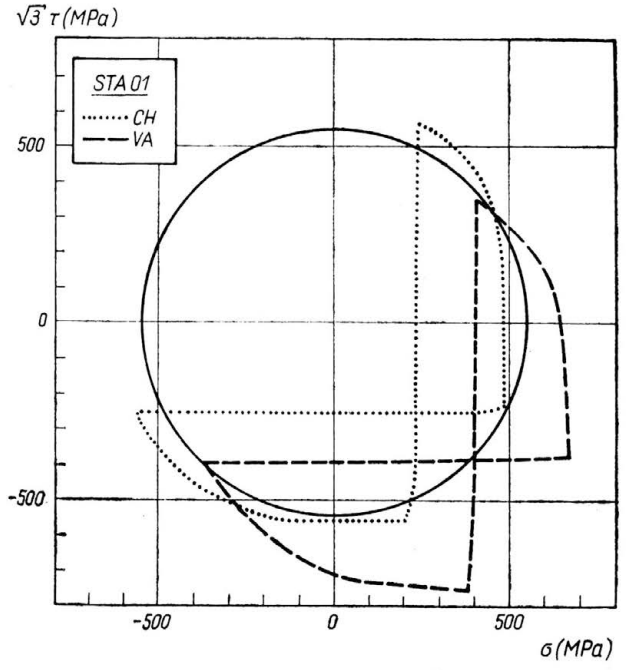

FIG. 10. Comparison of Chaboche's (CH) and Valanis' (VA) (σ,τ)-response to the fifth cycle of a strain controlled homogeneous axial torsional test, load path STA01 (stair test).

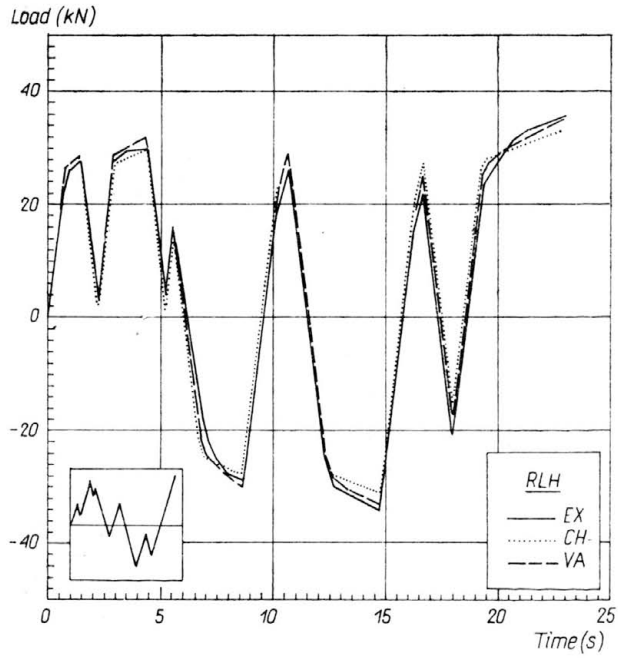

FIG. 11. Comparison between predicted load time behaviour of a smooth bar under random loading with experimental data (PE16: $\theta = 650°C$, $\dot{\varepsilon} = 4 \cdot 10^{-3}$ s^{-1}).

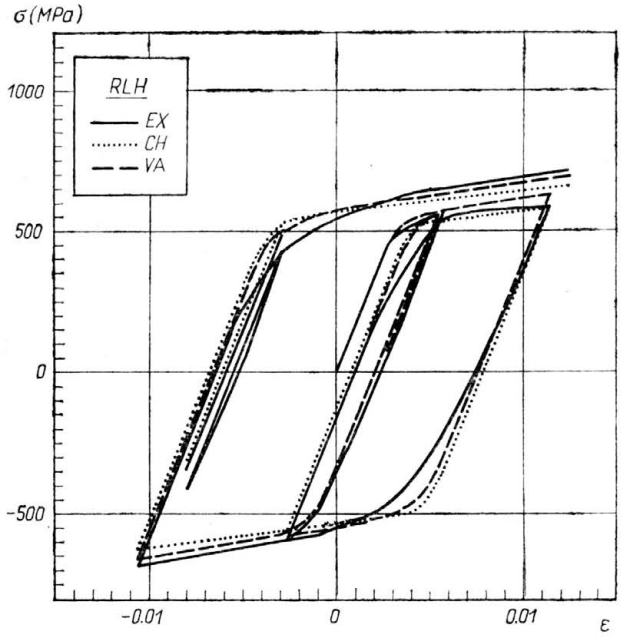

FIG. 12. Comparison between predicted stress-strain behaviour of a smooth bar under random loading with experimental data (PE16: $\theta = 650°C$, $\dot{\varepsilon} = 4 \cdot 10^{-3}$ s^{-1}).

test STA01 where the effective stress obtained from the Valanis model is 37% higher than that from the Chaboche model. The reason becomes clear from Fig. 10 where the fifth loading cycle is plotted. While the kinematic hardening reaches a state of saturation in the Chaboche model, it continues to increase in the Valanis model which is apparently due to Eq. (2 13). As no experimental data exist for the given material under this kind of loading, it cannot yet be decided which of the numerical simulations meets reality better than the other. In order to examine the model behaviour with respect to loading histories with varying strain amplitudes, a so-called random load history (RLH) has been considered. At first, some results obtained from a smooth specimen are shown in Figs. 11 and 12. In addition, Fig. 11 contains a sketch of the load history. The numerical predictions in form of a load vs. time (Fig. 11) and a stress/strain diagram (Fig. 12) have been compared with experimental data which are denoted by (EX). From these results it can be concluded that the examined material models give an adequate accuracy in predicting the material response at least for uniaxial loading conditions.

4.2. Inhomogeneous stress states (σ, τ)

Since all our structural components contain stress and strain concentrators as, for example, notches, it is more important to study the behaviour of notched specimens. But, unfortunately, the experimental techniques are not developed to measure the strain state at the root of sharp notches at high temperatures. Therefore, as yet we are not able to compare the FE results with experimental data, but we hope to overcome these experimental difficulties in the future. Hence a comparison can be made only on the basis of the two constitutive models.

As an example for a structural component, a circumferential notched cylindrical bar subjected to a loading program with variable strain amplitudes has been analyzed. The finite element idealization and the loading history (RLH) are given in Fig. 13, 70 axisymmetric 8-noded elements giving rise to 462 degrees of freedom. The finite element analysis based on the two constitutive models mentioned above has been carried out using the FE program ADINA [15]. The results are given in Figs. 14 to 21. Additional results can be found in [20, 21].

In Fig. 14 the material response close to the notch root characterized by the notch-opening stress-strain relationship is shown. The minor differences are based on the distinct slopes reflecting the different hardening behaviour of the two models. This is pointed out more clearly in Fig. 15 where the relation between the notch opening component of Cauchy's back stress tensor and the corresponding plastic strain component is plotted. Here, a very different description of the kinematical hardening behaviour can be observed. In order to answer the question for the correct modelling of the kinematical hardening behaviour, the calculated strain state or, alternatively, the displacement state at the notch root must be compared with experimental observations. In Fig. 16 the variation of the radial displacement taken at the net section of the bar in the course of the loading history is shown. This is a very sensitive measure of the hardening state at the notch root. Figure 17 exhibits the relationship to the corresponding outer loading.

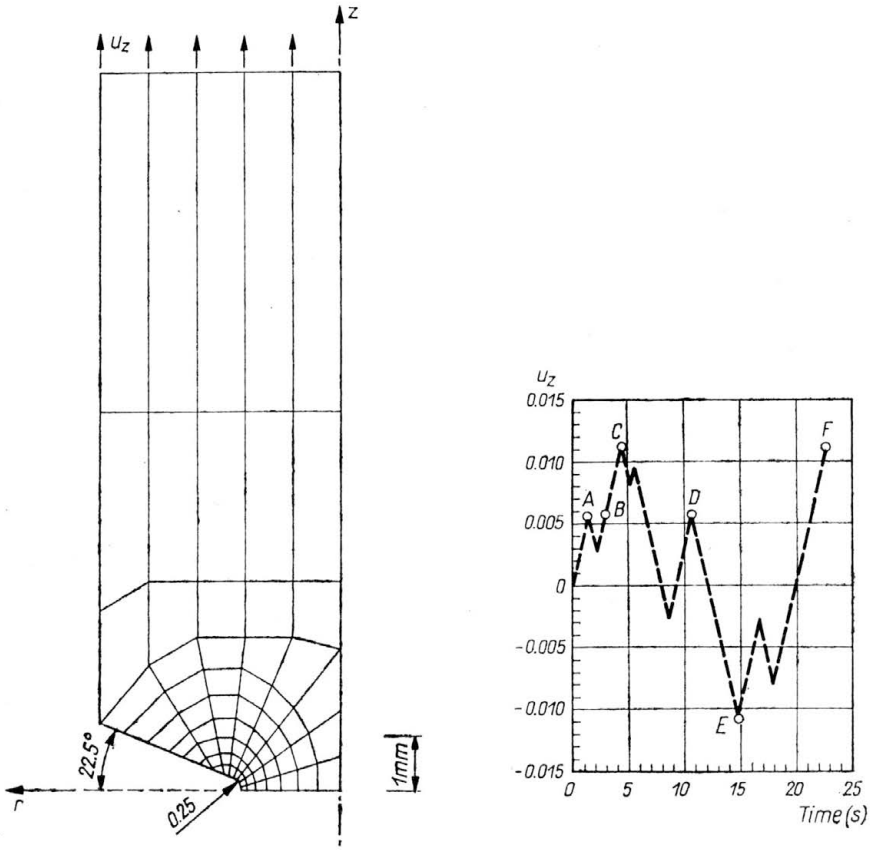

FIG. 13. Axisymmetric FE mesh, $K_t = 2.5$, random load history (RLH).

The notch opening stress distribution in the net section of the notched specimen referring to several load events of the loading program, denoted by A to F, are shown in Figs. 18 and 19. Both models show a very similar stress response. Comparing the load events A and C or F, an increase of the stress maximum can be detected. This is due to the transient hardening behaviour of the material used for these calculations. A comparison of the loading events A or B and D shows the influence of previous loading events, for example, an unloading situation which leads to a residual stress state.

Figures 20a, b and 21a, b show the variation of the multiaxial stress state calculated at the vicinity of the notch root in the principal stress space, i.e., in the deviatoric stress plane (Π-plane). It is seen that in the inelastic regime a nonproportional variation of the stress state takes place. Therefore, a nonproportional loading situation has to be considered locally, even when the outer loading is purely uniaxial. Therefore the question arises regarding the limitations of the concept of smooth specimen simulation.

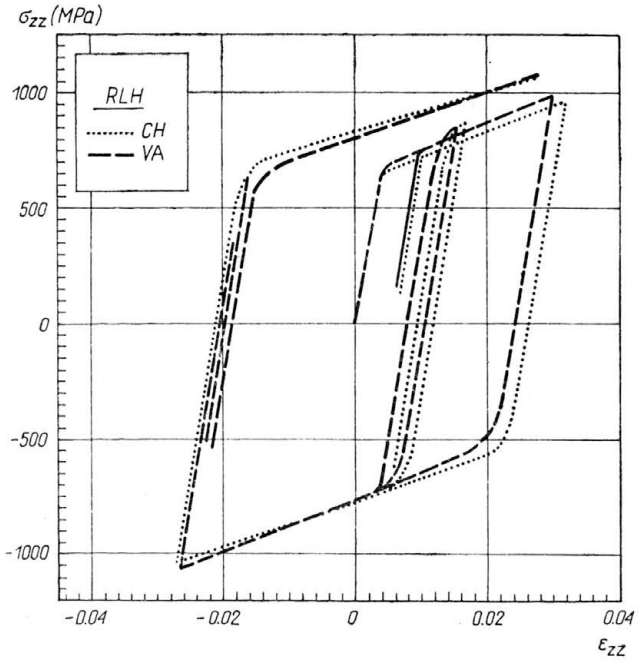

FIG. 14. Notch opening stress vs notch opening strain at the notch root.

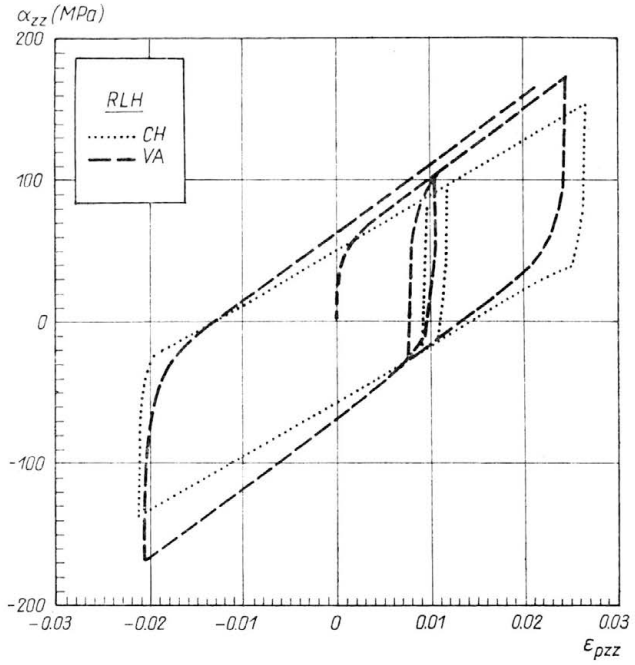

FIG .15. Notch opening component of the back stress tensor vs. corresponding plastic strain component.

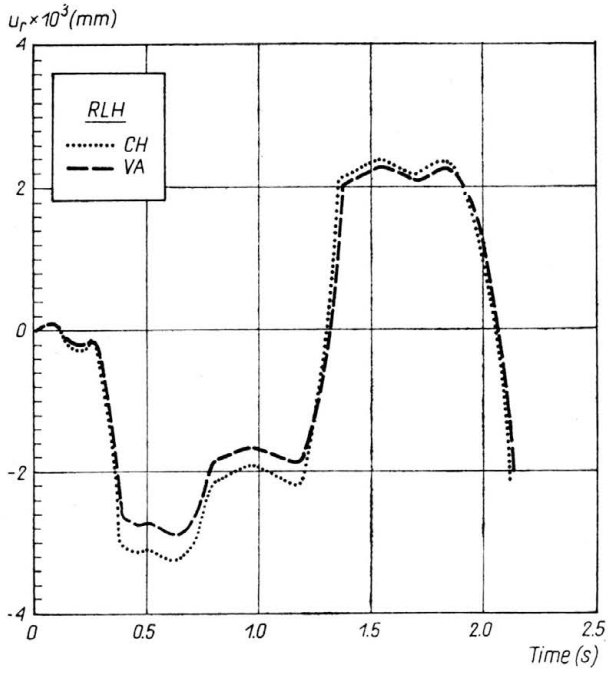

FIG. 16. Radial notch root displacement vs. time.

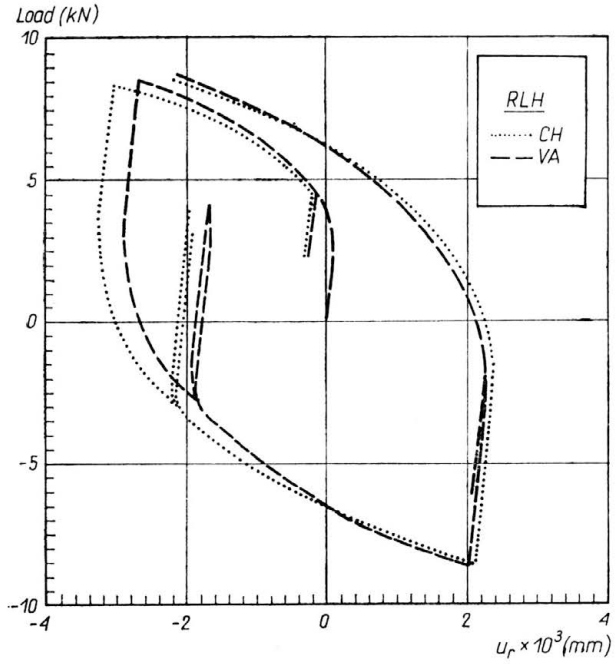

FIG. 17. Load vs radial notch root displacement.

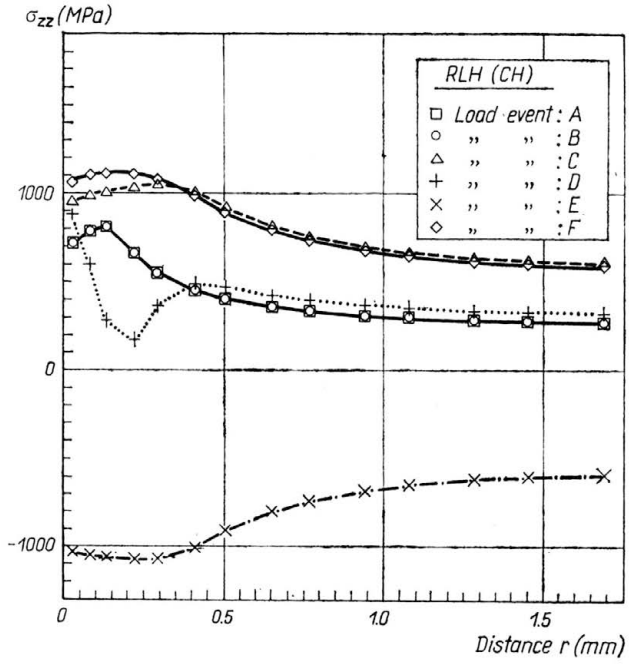

FIG. 18. Notch opening stress ahead of the notch root at different events of the loading program, Chaboche's model (CH).

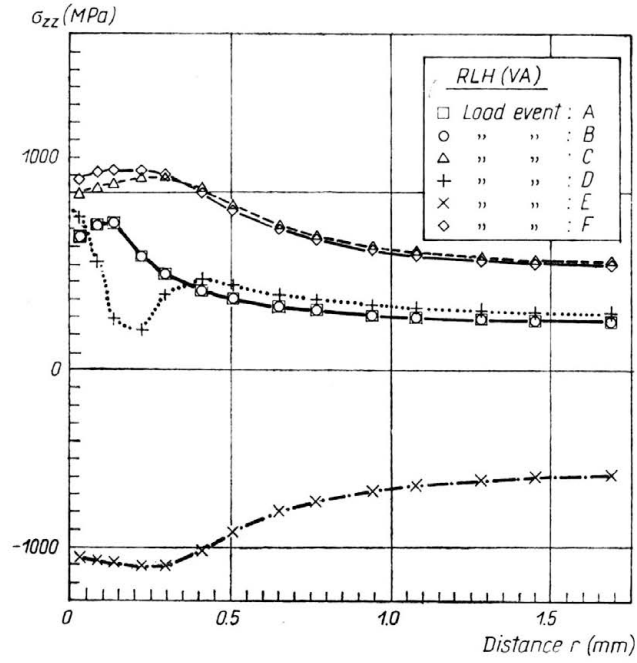

FIG. 19. Notch opening stress ahead of the notch root at different events of the loading program, Valanis' model (VA).

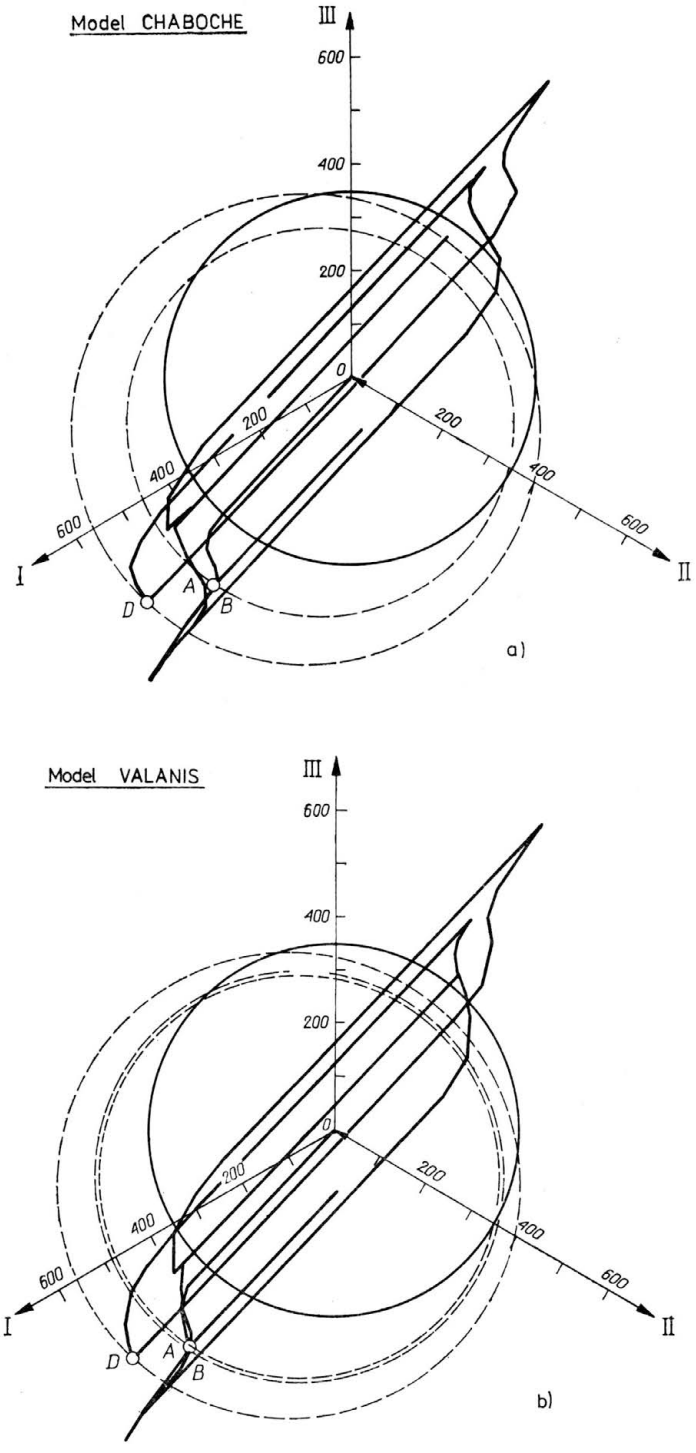

FIG. 20a, b. Variation of the multiaxial stress state at the notch root in the deviatoric stress plane (II-plane).

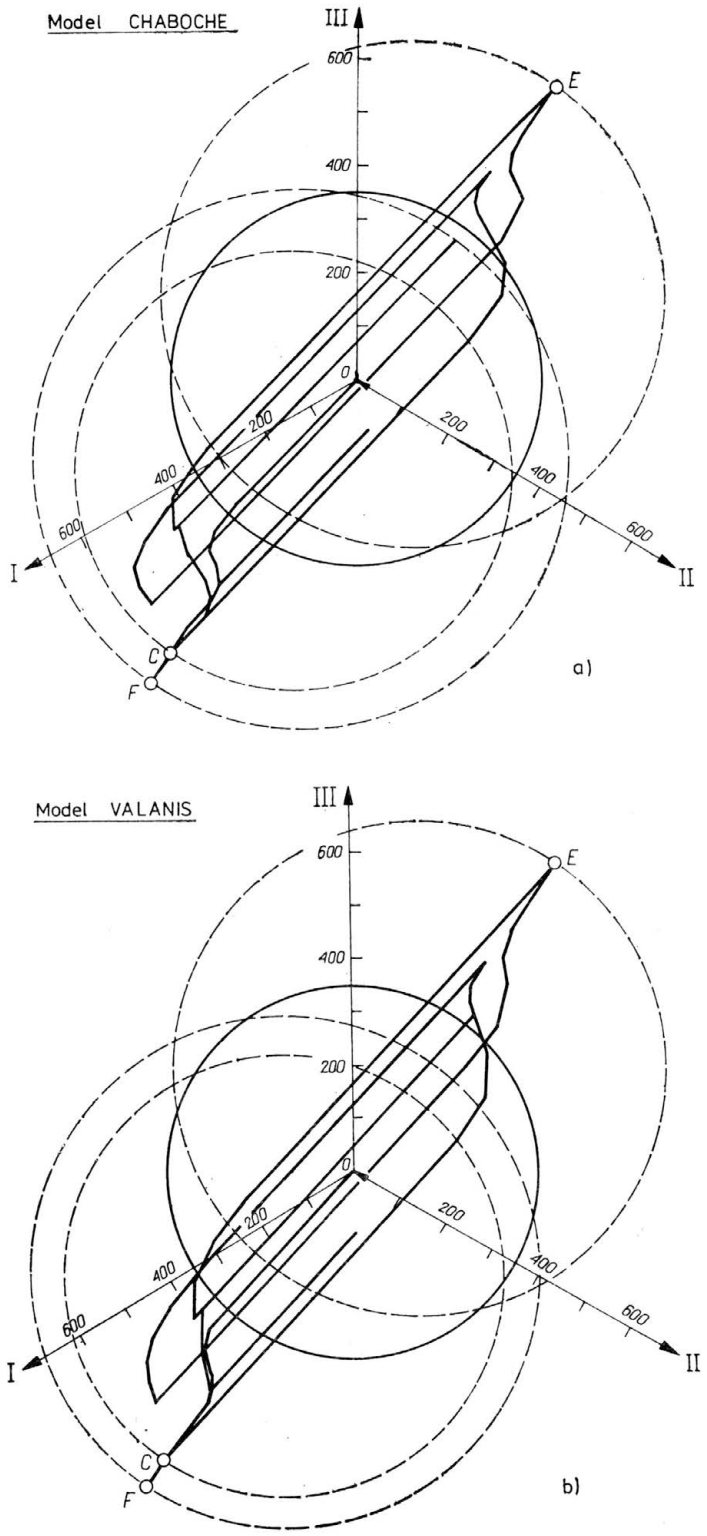

FIG. 21a,b. Variation of the multiaxial stress state at the notch root in the deviatoric stress plane (Π-plane).

5. Conclusions

According to an idea of Watanabe and Atluri, internal variable and internal time theories of plasticity may be unified by an appropriate choice of kernels in the latter. This has been verified not only with respect to analogies of equations but by a number of different numerical investigations of proportional and nonproportional, homogeneous and inhomogeneous stress and strain states. If the different material functions used in both concepts are adopted properly to experimental data, no significant differences will arise between the responses of the two constitutive models in most cases.

Some exceptions have been found concerning the kinematic hardening behaviour of the investigated models. First, one of the stair tests with an extremely eccentric load path in the strain space (STA01) showed increasing differences in strain hardening with continuing cycles because the Valanis model did not reach a saturation state as the Chaboche model did. Second, the z- component of the back-stress tensor, α_{zz}, in dependence on the plastic strain differed between the models for a notched bar.

The dependency of strain hardening on the kind of load paths during the tests which has been observed experimentally does not seem to be predicted adequately by both models though some effects could be realized numerically. As corresponding experimental data are missing for the investigated steel, no final conclusion can be drawn.

A satisfactory measure of the degree of nonproportionality of a given load path has not yet been found. The definition of Φ^* given by McDowell turned out not to differentiate between different stair tests. As it refers to the plastic strain, it becomes material-dependent and cannot characterize the load path itself.

Additional experiments are necessary for the same nonproportional tests investigated numerically in the present paper. Besides biaxial tests under homogeneous tension and torsion, uniaxial experiments on notched bars will give valuable information about multiaxial states induced by the notch if the radial displacement at the notch root can be measured.

References

1. J. L. CHABOCHE, K. DANG VAN and G. CORDIER, *Modellization of the strain memory effect on the cyclic hardening of 316 stainless steel*, Trans. 5th SMiRT, Berlin, FR Germany, L 11/3, 1979.
2. J. L. CHABOCHE and G. ROUSSELIER, *On the plastic and viscoplastic constitutive equations, Part I. Rules developed with internal variable concept. Part II. Application of internal variable concept to the 316 stainless steel*, J. Press. Vess. Techn., **105**, 153–164, 1983.
3. K. C. VALANIS, *A theory of viscoplasticity without a yield surface, Part I. General theory, Part II. Application to mechanical behaviour of metals*, Arch. Mech., **23**, 511–551, 1971.
4. K. C. VALANIS, *Fundamental consequence of a new intrinsic time measure plasticity as a limit of the endochronic theory*, Arch. Mech., **32**, 171–191, 1980.
5. K. C. VALANIS and J. FAN, *Endochronic analysis of cyclic elasto-plastic strain fields in a notched plate*, J. Appl. Mech., **59**, 789–794, 1983.
6. K. C. VALANIS and J. FAN, *Experimental verification of endochronic plasticity in spatially varying strain fields*, in: Plasticity Today (ed. A. SAWCZUK and G. BIANCHI), Elsevier Appl. Sc. Publ., London–New York 1985.
7. O. WATANABE and S. N. ATLURI, *A new endochronic approach to computational elastoplasticity. Example of a cyclically loaded cracked plate*, J. Appl. Mech., **52**, 857–864, 1985.

8. O. WATANABE and S. N. ALTURI, *Internal time, general internal variable and multiyield surface theories of plasticity and creep: a unification of concepts*, Int. J. Plasticity, **2**, 37–67, 1986.
9. H. S. LAMBA and O. M. SIDEBOTTOM, *Cyclic plasticity for non-proportional paths, Part I. Cyclic hardening, erasure of memory, and subsequent strain hardening experiments, Part II. Comparison with predictions of three incremental plasticity models*, J. Engng. Mat. Tech., **100**, 96–111, 1978.
10. K. KANAZAWA and K. J. MILLER, *Cyclic deformation of 1% Cr Mo V steel under out of phase loads*, Fatigue Eng. Mat. and Struct. **2**, 217–228, 1979.
11. G. CAILLETAUD, H. KACZMAREK and H. POLICELLA, *Some elements on multiaxial behaviour of 316 L stainless steel at room temperature*, Mech. Materials, **3**, 333–347, 1984.
12. D. L. MCDOWELL, *An experimental study of the structure of constitutive equations for non-proportional cyclic plasticity*, J. Engng. Mat. Tech., **107**, 307–315, 1985.
13. E. TANAKA, S. MURAKAMI and M. OOKA, *Effects of strain path shapes on non-proportional cyclic plasticity*, J. Mech. Phys. Solids, **33**, 559-575, 1985.
14. A. BENALLAL and D. MARQUIS, *An experimental investigation of cyclic hardening of 316 stainless steel, under complex multiaxial loadings*, Trans. 9th SMiRT, Vol. L, 385–393. Lausanne, Switzerland, 1987.
15. K. J. BATHE, *ADINA — A finite element program for automatic dynamic incremental nonlinear analysis*, Report AE 84-1, ADINA-Engineering, Inc., Watertown, USA 1984.
16. S. P. SCHOLZ, *Numerische Untersuchungen zum Verhalten des Hochtemperaturwerkstoffes Nimonic PE16 unter monotoner und zyklischer Belastung bei Verwendung verschiedener plastischer und viskoplastischer Materialmodelle*, Master Thesis, TUB/BAM, Berlin 1986.
17. A. JULA, *Numerische Behandlung des Verhaltens eines Hochtemperaturwerkstoffes unter zyklischer Belastung mit der endochronen Plastizitätstheorie*, Master Thesis, TUB/BAM, Berlin 1987.
18. D. L. MCDOWELL, *An evaluation of recent developments in hardening and flow rules for rate-independent, non-proportional cyclic plasticity*, J. Appl. Mech., **54**, 323–334, 1987.
19. J. OLSCHEWSKI and S. P. SCHOLZ, *Numerische Untersuchungen zum Verhalten des Hochtemperaturwerkstoffes Nimonic PE16 unter monotoner und zyklischer Belastung bei Verwendung plastischer und viskoplastischer Materialmodelle*, BAM Forschungsbericht 139, Berlin 1987.
20. J. OLSCHEWSKI, *Inelastic stress-strain behaviour of cyclic loaded notched specimens*, Trans 9th SMiRT, Vol. L, 395–401, Lausanne, Switzerland 1987.
21. J. OLSCHEWSKI, *Inelastic stress-strain behaviour of cyclic loaded notched specimens*, Proc. 2nd Int. Conf. on Low Cycle Fatigue and Elasto-Plastic Behaviour of Metals, DVM, Munich, FR Germany, 352–537, 1987.

BUNDESANSTALT FÜR MATERIALFORSCHUNG UND-PRUFÜNG (BAM), BERLIN.

Received January 6, 1988.